Moiré Materials

and

Fractional Chern Insulators

Lecture notes of

Titus Neupert

MaNEP Winter School

Saas Fee 2025

Contents

1 Moiré materials 1
- 1.1 Graphene and Dirac equation . . . 1
- 1.2 Structure and electronic structure of TMDs . . . 4
- 1.3 Twisting . . . 5
  - 1.3.1 Twisting graphene . . . 6
  - 1.3.2 Twisting TMDs . . . 9

2 Fractional Chern Insulators (FCIs) 10
- 2.1 Fractional Quantum Hall E□ect (FQHE) . . . 10
- 2.2 Fractional Chern Insulators (FCIs) . . . 12

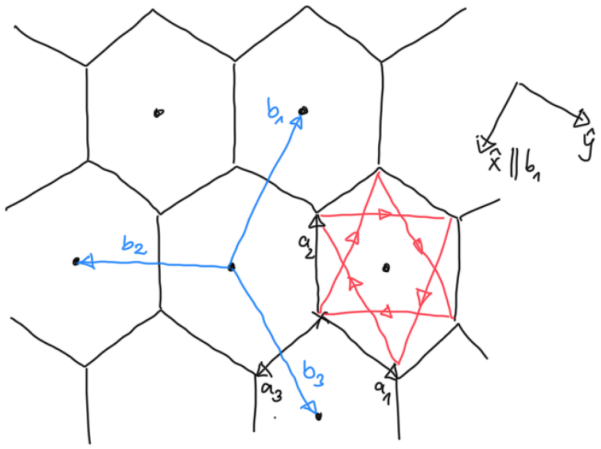

Figure 1: Honeycomb lattice, with definition of nearest/neighbor vectors a_1, a_2, a_3 and lattice vectors b_1, b_2, b_3. Shown in red are the directed, complex next nearest-neighbor hoppings present in the Haldane model.

1 Moiré materials

1.1 Graphene and Dirac equation

Following Haldane[1], we consider an electronic system with nearest neighbour (NN) and next nearest neighbour (NNN) hopping on a honeycomb lattice, as shown in Fig. 1. There are 3 nearest neighbours, corresponding to the vectors a_1, a_2, a_3 and 6 next nearest neighbours, for hopping between sites on the same sublattice (A or B), corresponding to the lattice vectors

$$\begin{aligned} b_1 &= a_2 \quad a_3, \\ b_2 &= a_3 \quad a_1, \\ b_3 &= a_1 \quad a_2, \\ b_4 &= \quad b_1, \\ b_5 &= \quad b_2, \\ b_6 &= \quad b_3. \end{aligned}$$

With the spinors (in k space)

$$\begin{pmatrix} \psi_{\boldsymbol{k},\mathrm{A}} \\ \psi_{\boldsymbol{k},\mathrm{B}} \end{pmatrix} \tag{1}$$

[1] F.D.M. Haldane, *Model for a quantum Hall e ect without Landau levels: Condensed-matter realization of the "parity anomaly"*, Phys. Rev. Lett. 61(18), 2015–2018 (1988).

describing the electrons on the two sublattices A and B, we consider the Hamiltonian

$$\begin{aligned}\widehat{H} &= t_1 \sum_{i=1}^{3} \Big[\cos(k \;\; a_i)\sigma_1 + \sin(k \;\; a_i)\sigma_2 \Big] \\ &\quad + 2t_2 \cos\phi \Big(\sum_{i=1}^{3} \cos(k \;\; b_i) \Big) \sigma_0 \\ &\quad + \Big[M \;\; 2t_2 \sin\phi \Big(\sum_{i=1}^{3} \sin(k \;\; b_i) \Big) \Big] \sigma_3 .\end{aligned} \tag{2}$$

The parameters in this Hamiltonian are:

- t_1, describing NN hopping. This parameter delivers the main band structure of graphene.
- t_2, describing NNN hopping with a directed flux ϕ. The choice $\phi = 0$ describes graphene, whereas $\phi \neq 0$ provides Haldane's model.
- M, describing a staggered SL potential (Semeno term). The choice $M \;!\; 1$ delivers two ("boring") flat bands localized on either sublattice.

The symmetries of the system are:

- Graphene (with only t_1): C_{6v} and time reversal symmetry (TRS).
- $t_2 \neq 0$ with $\phi \neq 0, \pi$ breaks TRS.
- $M \neq 0$ breaks inversion symmetry and $C_{6v} \;!\; C_{3v}$; $M \neq 0$ alone preserves TRS.

Special points in k-space are K and K' at the corners of the Brillouin zone (see Fig. 2). Their coordinates k_α [with $\alpha = +1$ (1) for K (K')] satisfy

$$(k_\alpha \;\; a_1, k_\alpha \;\; a_2, k_\alpha \;\; a_3) = \sigma\Big(0, \frac{2\pi}{3}, \;\; \frac{2\pi}{3}\Big), \qquad k_\alpha \;\; b_i = \frac{2\pi}{3}\alpha \tag{3}$$

for some permutation σ.

The low-energy theory is obtained by a $k \;\; p$ perturbation expansion around K and K'. With

$$\begin{aligned} \cos(0) \;\; &' \;\; 1, \\ \sin(0 + \;\; k \;\; a_1) \;\; &' \;\; k \;\; a_1, \\ \cos\big(\frac{2\pi}{3} + \;\; k \;\; a_2\big) \;\; &' \;\; \frac{1}{2} \;\; \frac{\sqrt{3}}{2} \;\; k \;\; a_2, \\ \sin\big(\frac{2\pi}{3} + \;\; k \;\; a_2\big) \;\; &' \;\; \frac{\sqrt{3}}{2} \;\; \frac{1}{2} \;\; k \;\; a_2, \\ \cos\big(\;\; \frac{2\pi}{3} + \;\; k \;\; a_3\big) \;\; &' \;\; \frac{1}{2} + \frac{\sqrt{3}}{2} \;\; k \;\; a_3, \\ \sin\big(\;\; \frac{2\pi}{3} + \;\; k \;\; a_3\big) \;\; &' \;\; \frac{\sqrt{3}}{2} \;\; \frac{1}{2} \;\; k \;\; a_3 \end{aligned} \tag{4}$$

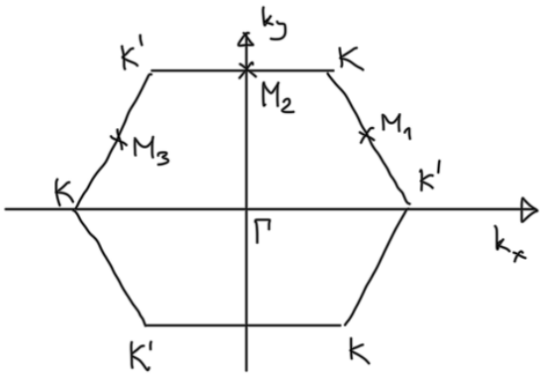

Figure 2: The first Brillouin zone of a triangular/hexagonal lattice in k-space. High-symmetry points are labeled, the three M points M_1, M_2, M_3 are equivalent with sixfold rotation symmetry (or threefold rotation and time reversal). The K and K' point are equivalent under time-reversal or twofold rotation.

we obtain

$$\sum_{i=1}^{3} \cos(\boldsymbol{k} \cdot \boldsymbol{a}_i) = \frac{\sqrt{3}}{2} \quad \boldsymbol{k} \cdot (\boldsymbol{a}_3 - \boldsymbol{a}_2), \tag{5}$$

$$\sum_{i=1}^{3} \sin(\boldsymbol{k} \cdot \boldsymbol{a}_i) = \frac{1}{2} \quad \boldsymbol{k} \cdot (\boldsymbol{a}_1 - \boldsymbol{a}_2 - \boldsymbol{a}_3). \tag{6}$$

Since $\boldsymbol{a}_3 - \boldsymbol{a}_2$ is in k_x-direction with magnitude $2a/\sqrt{3}$ and $\boldsymbol{a}_1 - \boldsymbol{a}_2 - \boldsymbol{a}_3$ in k_y-direction with magnitude $2a$ (with a the NN distance), the effective Hamiltonian is

$$\widehat{H}_{\text{eff},\alpha} = t_1 a(k_x \sigma_1 + \alpha k_y \sigma_2) + m_\alpha \sigma_3, \tag{7}$$

where

$$m_\alpha = M - 3\sqrt{3}\alpha t_2 \sin\phi, \tag{8}$$

we redefined the momenta ($\boldsymbol{k} \to \boldsymbol{k}$) and $\alpha = 1$ (-1) for the perturbation expansion around K (K'). The Pauli matrices $\sigma_1, \sigma_2, \sigma_3$ mutually anticommute, therefore (7) is the Hamiltonian of a Dirac equation with mass term m_α. The energy bands are then given by

$$E_{\boldsymbol{k},\alpha,\pm} = \pm\sqrt{(t_1 a)^2(k_x^2 + k_y^2) + m_\alpha^2}. \tag{9}$$

The competing masses M and $t_2 \sin\phi$ lead to different phases, as shown in the phase diagram in Fig. 3, where the phase boundaries correspond to gap closings.

The phases can be distinguished by the Chern number C, a topological invariant, taking different integer values in the different phases. The Chern number is defined by

$$C = \frac{1}{2\pi} \int d^2k F_{xy}, \tag{10}$$

where F_{xy} is the Berry curvature, with the general definition

$$F_{xy} = \mathrm{i}\left(\hbar\partial_{k_x} u_{\boldsymbol{k}} | \partial_{k_y} u_{\boldsymbol{k}}\rangle - \hbar\partial_{k_y} u_{\boldsymbol{k}} | \partial_{k_x} u_{\boldsymbol{k}}\rangle\right). \tag{11}$$

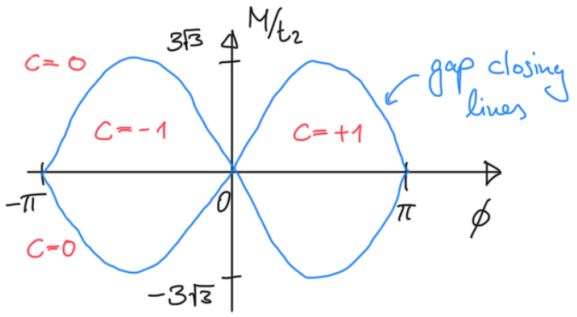

Figure 3: Phase diagram of the Haldane model

If $H(k) = d(k)$, with = $(\sigma_1, \sigma_2, \sigma_3)$, we can use

$$\begin{aligned} C &= \frac{1}{2\pi}\int d^2k\, \frac{d\ (\partial_{k_x} d\ \ \partial_{k_y} d)}{2jdj^3} \\ &= \frac{1}{2\pi}\frac{1}{2}\int d^2k\, \frac{\sum_{\alpha=\ 1} m_\alpha \alpha t_1^2 a^2}{\sqrt{t_1^2 a^2 k^2 + m_\alpha^2}^3}, \end{aligned} \tag{12}$$

since

$$\partial_{k_x} d = \begin{pmatrix} t_1 a \\ 0 \\ 0 \end{pmatrix}, \qquad \partial_{k_y} d = \begin{pmatrix} 0 \\ \alpha t_1 a \\ 0 \end{pmatrix}. \tag{13}$$

Therefore,

$$\begin{aligned} C &= \frac{1}{2\pi}\frac{1}{2}\frac{1}{t_1 a} 2\pi \sum_{\alpha=\ 1} m_\alpha \alpha \underbrace{\int dk\, k\, \frac{1}{\sqrt{k^2 + \left(\frac{m_\alpha}{t_1 a}\right)^2}^3}}_{\frac{1}{\left|\frac{m_\alpha}{t_1 a}\right|}} \\ &= \frac{1}{2}\sum_{\alpha=\ 1} \mathrm{sgn}(m_\alpha \alpha) \qquad (14) \\ &= \begin{cases} 0, & M \text{ large}, \\ 1, & t_2 \sin(\phi) \text{ large}. \end{cases} \qquad (15) \end{aligned}$$

As a physical consequence, the o□-diagonal conductivity is quantized, $\sigma_{xy} = \frac{e^2}{h} C$.

1.2 Structure and electronic structure of TMDs

Examples of TMDs are $MoTe_2$, WTe_2, $MoSe_2$, WSe_2, MoS_2, WS_2. They are van der Waals materials, exfoliatable and come in di□erent structures, some of them meta-stable. The nomenclature is as follows:

- H . . . hexagonal (TM atom coordination)
  T . . . trigonal
  M . . . monoclinic
- nH / nT / nM: n layers in 3D unit cell

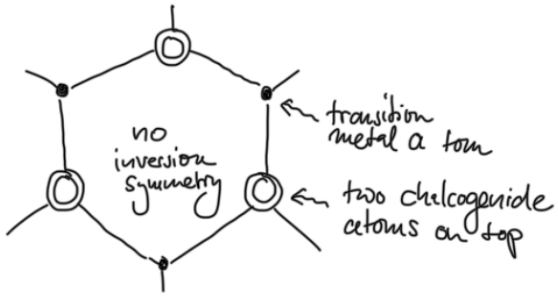

Figure 4: Absence of inversion symmetry in 1H-TMDs.

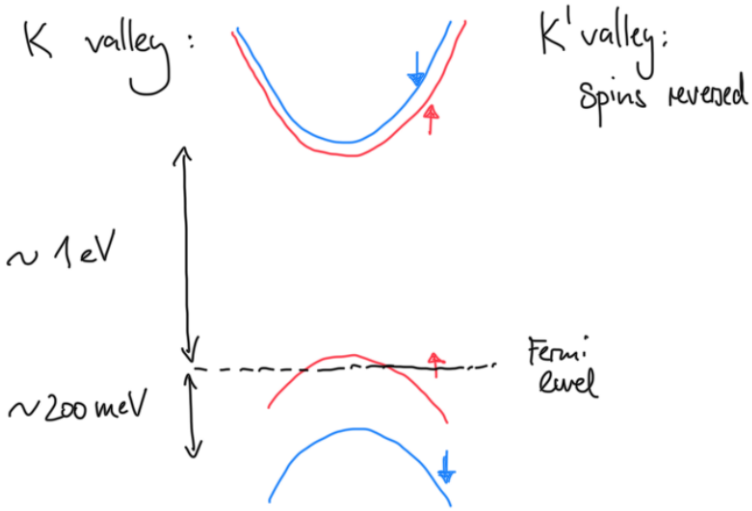

Figure 5: Schematic electronic structure in each valley in TMDs.

- primes for different space groups: 1T, 1T',...

Here we consider the structure 1H, i.e., hexagonal monolayer TMDs. They have a large SOC compared to graphene and large M, due to the broken SL symmetry (cf. Fig. 4). As consequence a so-called "valley Hall effect" arises, as depicted in Fig. 5 (remark that in the K'-valley the arrows are reversed, due to TRS): excitations $in\ one\ valley$ have a Hall response, described by the effective Hamiltonian

$$\widehat{H}_{\text{e}\ ,\alpha} = t_1 a(k_x\sigma_1 \quad \alpha k_y\sigma_2) + M\sigma_3 + \begin{pmatrix} {}^{c} & 0 \\ 0 & {}_{v} \end{pmatrix} \alpha\widehat{S}_3, \tag{16}$$

where $_c$ ($_v$) are the SOC strengths. The matrix in the last term acts on the degrees of freedom of the matrices, while $\widehat{S}_3$ is the z-component of the spin operator.

1.3 Twisting

Twisting is fundamentally different in graphene and TMDs, since the starting points are different: massless vs. massive. For graphene this gives rise to a "magic angle". For small angles, each valley is considered separately (cf. Fig. 6).

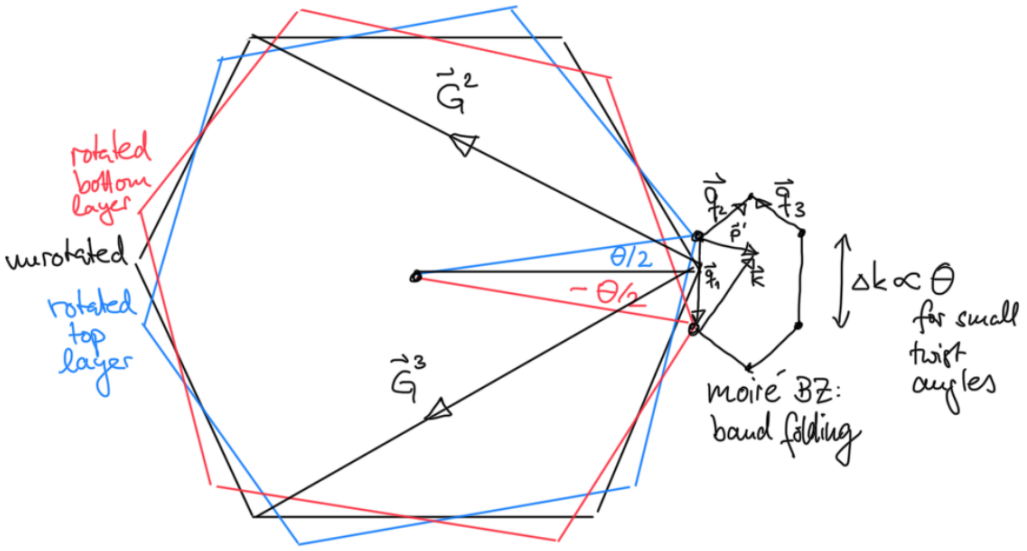

Figure 6: Construction of the moiré Brillouin zone in twisted bilayer materials.

1.3.1 Twisting graphene

The e□ective Hamiltonian (per layer graphene) is

$$h_{\boldsymbol{k}}(\theta) = v_{\boldsymbol{k}} \begin{pmatrix} 0 & e^{\mathrm{i}(\theta_{\boldsymbol{k}} - \theta)} \\ e^{\mathrm{i}(\theta_{\boldsymbol{k}} - \theta)} & 0 \end{pmatrix}, \tag{17}$$

i.e., the same as before, where $\theta_{\boldsymbol{k}}$ is the angle of the momentum $\boldsymbol{k}$ relative to the x-axis. With two layers the intralayer Hamiltonian is

$$\widehat{H}_0 = |1\rangle\langle 1| h(\theta/2) + |2\rangle\langle 2| h(-\theta/2), \tag{18}$$

where $|j\rangle\langle j|$ is the projector on the j-th layer.

The interlayer hopping is described by the matrix elements

$$T^{\alpha\beta}_{\boldsymbol{k}\boldsymbol{p}'} = \langle \psi^{(1)}_{\boldsymbol{k},\alpha} | H_T | \psi^{(2)}_{\boldsymbol{p}',\beta} \rangle, \tag{19}$$

where the upper index refers to the layer (1 or 2), α, β to the sublattice (A or B) and $\boldsymbol{p}' = M(\theta)\boldsymbol{p}$, with $M(\theta)$ the rotation by θ. This includes contributions from all unit cells in reciprocal space but decreases rapidly when $qd_z > 1$, with d_z the layer separation ($d_z \gtrsim 2a$), due to the 3D separation $R = \sqrt{r^2 + d_z^2}$. Then, approximately, only 3 BZ adjacent to the Dirac point contribute significantly:

$$T^{\alpha\beta}(\boldsymbol{r}) = \omega \sum_{j=1}^{3} e^{\mathrm{i}\boldsymbol{q}_j \cdot \boldsymbol{r}} T^{\alpha\beta}_j, \tag{20}$$

where the $\boldsymbol{q}_j$'s are shown in Fig. 6, ω is the hopping energy ($\omega \simeq 110$meV for non-twisted graphene) and

$$T_1 = \begin{pmatrix} 1 & 1 \\ 1 & 1 \end{pmatrix}, \qquad T_2 = \begin{pmatrix} e^{\mathrm{i}\phi} & 1 \\ e^{\mathrm{i}\phi} & e^{\mathrm{i}\phi} \end{pmatrix}, \qquad T_3 = \begin{pmatrix} e^{\mathrm{i}\phi} & 1 \\ e^{\mathrm{i}\phi} & e^{\mathrm{i}\phi} \end{pmatrix}, \tag{21}$$

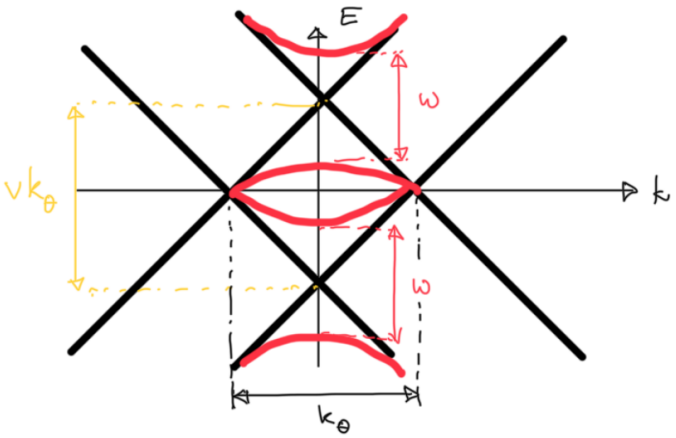

Figure 7: Intuition for the parameter $\alpha = \frac{\omega}{vk_\theta}$ that determines the magic angles in twisted bilayer graphene can be obtained from comparing the hybridization energy scale with the relative displacement of the Dirac cones in momentum space due to the rotation.

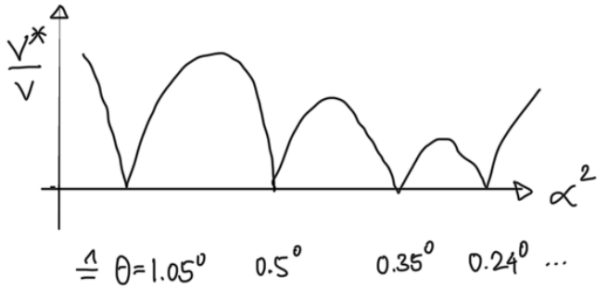

Figure 8: Qualitative evolution of the e□ective velocity in the moiré bands with the twisting parameter α. v = 0 defines the magic angles.

with $\phi = 2\pi/3$.

Numerical diagonalization of this Hamiltonian keeping vectors up to $\omega/\sim v$ requires matrices of dimension $10\theta^{-2}$ (θ in degrees), compared to $10^4\theta^{-2}$ for a full diagonalization. It is appropriate to use a single parameter $\alpha = \omega/(vk_\theta)$, with $k_\theta = j\boldsymbol{q}_i j$. The intuition behind this choice is sketched in Fig. 7.

The experiments do not show a monotonical narrowing with θ, but the appearence of so-called "magic angles" (at $\theta = 1.05$ and other values), at which the Dirac point velocity v vanishes, as shown in Fig. 8.

To reproduce these results, a NN truncation in momentum hopping gives the Hamiltonian

$$\widehat{H}_{\boldsymbol{k}} = \begin{bmatrix} h_{\boldsymbol{k}}(\theta/2) & T_1 & T_2 & T_3 \\ T_1^y & h_{\boldsymbol{k}+\boldsymbol{q}_1}(-\theta/2) & 0 & 0 \\ T_2^y & 0 & h_{\boldsymbol{k}+\boldsymbol{q}_2}(-\theta/2) & 0 \\ T_3^y & 0 & 0 & h_{\boldsymbol{k}+\boldsymbol{q}_3}(-\theta/2) \end{bmatrix}. \tag{22}$$

The $\boldsymbol{k}\cdot\boldsymbol{p}$ expansion around $\boldsymbol{k} = 0$ results in two bands with e□ective Hamiltonian

$$\widehat{H}_{\mathrm{e},\boldsymbol{k}} = v\,\boldsymbol{k}, \tag{23}$$

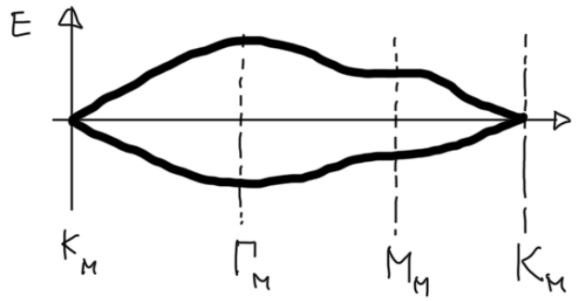

Figure 9: Moiré energy bands with a Dirac point at K_M.

with

$$v = v\frac{1 - 3\alpha^2}{1 + 6\alpha^2} \sim v(1 - 9\alpha^2) \to 0 \quad \text{for } \alpha \to 1/3. \tag{24}$$

Per valley there are 4 bands which are spin degenerate, for a total of 8 bands. For a better approximation one considers matrices of the form

$$T_i = \omega_0\Big[\text{diagonal}\Big] + \omega_1\Big[\text{o}\square\text{-diagonal}\Big], \tag{25}$$

where the diagonal (o□-diagonal) matrix describes AA (AB) hopping. This results in a Dirac point near K_M for $\omega_0 \neq \omega_1$, as shown in Fig. 9. Furthermore, all bands are anomalous[2], with p-h symmetry taken into account, not lattice regularizable at any cuts. The flat bands are topologically fragile, or, with p-h symmetry, topologically stable, and hence not lattice regularizable.

In the Chern band basis[3], per valley and per spin, one has to consider two Chern bands with $C = -1$, in the limit where the dispersion is neglected. In total, one obtains four $C = +1$-bands (2 spins $\times$ 2 valleys) and four $C = -1$-bands. In the chiral limit the $U(4) \times U(4)$ symmetry holds and $\omega_0 = 0$. In the nonchiral-flat limit (spectrally flat, but $\omega_0, \omega_1 \neq 0$), the $U(4)$ spin-valley symmetry holds. As a consequence, the option with the smallest C is favorized for each $\nu = -4, -3, \ldots, 3, 4$. It follows that $C = 0$ for ν even and $C = -1$ for ν odd, representing all $U(4)$ fm ground states. Switching the dispersion on, only the $U(2) \times U(2)$ symmetry remains, giving the favorized states:

- $C = 0$ states for ν even: intervalley-coherent,
- $C = -1$ states for $\nu = -1$: partially intervalley-coherent,
- $C = -1$ states for $\nu = -3$: valley-polarized.

But, due to strain and substrate, the integer filling GS is an incommensurate Kakulé spiral (IKS) state, with TRS, broken translational symmetry and intervalley coherence.

In the strong coupling approach, one considers the Wannier orbitals, which have a fidget spinner form (cf. Fig. 10). The strong coupling locks the u, v_1, v_2, v_3 interactions to

$$u : v_1 : v_2 : v_3 = 3 : 2 : 2 : 1, \tag{26}$$

associated to "cluster charging interaction" with VBS ground states.

[2] Zhi-Da Song, Biao Lian, Nicolas Regnault, and B. Andrei Bernevig, *Twisted bilayer graphene. II. Stable symmetry anomaly*, Phys. Rev. B 103, 205412 (2021).

[3] Biao Lian, Zhi-Da Song, Nicolas Regnault, Dmitri K. Efetov, Ali Yazdani, and B. Andrei Bernevig, *Twisted bilayer graphene. IV. Exact insulator ground states and phase diagram*, Phys. Rev. B 103, 205414 (2021).

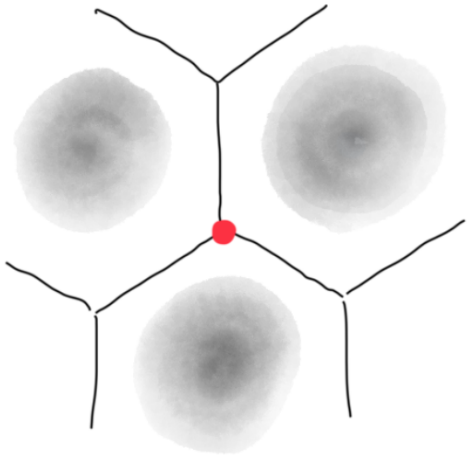

Figure 10: The Wannier orbitals of the states that make up the moiré bands take a fidget spinner shape.

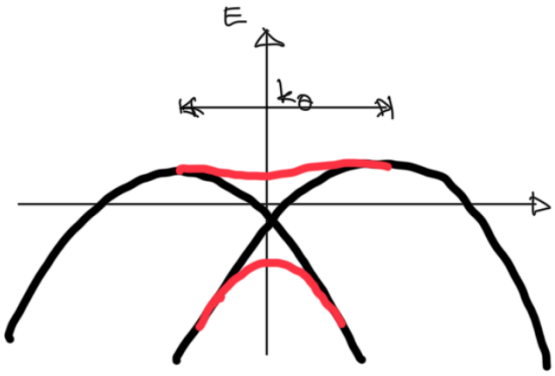

Figure 11: Qualitative electronic structure of twisted TMDs.

1.3.2 Twisting TMDs

The treatment is almost the same as in graphene, just with a different single particle Hamiltonian (with dispersion $\propto k^2$), with only one band per valley and no spin degeneracy (cf. Fig. 11). Furthermore, there is no "magic angle". The effective Hamiltonian has the form

$$\hat{H}_{\mathrm{e}} = \begin{bmatrix} \frac{1}{2m}\left(k - \frac{\boldsymbol{q}_1}{2}\right)^2 + \ldots & T(r) \\ T^{\dagger}(r) & \frac{1}{2m}\left(k + \frac{\boldsymbol{q}_1}{2}\right)^2 + \ldots \end{bmatrix} \tag{27}$$

This deliver bands with equal valley and spin Chern numbers that change with the angle θ and leads to a realization of the QSHE.

2 Fractional Chern Insulators (FCIs)

2.1 Fractional Quantum Hall Effect (FQHE)

We consider the Landau levels Hamiltonian

$$\widehat{H} = \frac{1}{2m}\Big(\widehat{p} \quad eA(\widehat{r})\Big)^2. \tag{28}$$

Using the ladder operators, with the magnetic length $\ell = \sqrt{\frac{1}{eB}}$,

$$\widehat{a}^\dagger = \frac{\ell}{\sqrt{2}}\left[(\widehat{p}_x + eA_x + i(\widehat{p}_y + eA_y)\right], \tag{29}$$

we obtain

$$\widehat{H} = \omega_c\Big(\widehat{a}^\dagger\widehat{a} + \frac{1}{2}\Big), \tag{30}$$

where $\omega_c = \frac{eB}{m}$ is the cyclotron frequency (and $\hbar = 1$). We can define a second set of ladder operators which commutes with first set,

$$\widehat{b}^\dagger = \frac{1}{\sqrt{2}\ell}\left[\widehat{r}_x \quad \ell^2(\widehat{p}_y + eA_y) \quad i[\widehat{r}_y + \ell^2(\widehat{p}_x + eA_x)]\right]. \tag{31}$$

Both sets satisfy a bosonic algebra,

$$[\widehat{a}, \widehat{a}^\dagger] = 1, \qquad [\widehat{b}, \widehat{b}^\dagger] = 1. \tag{32}$$

Choosing the symmetric gauge,

$$A = \frac{1}{2}(\ \ B\widehat{r}_y, B\widehat{r}_x, 0), \tag{33}$$

we obtain the eigenfunctions in the lowest Landau level (LLL, with $n_a = 0$),

$$\langle r|0, n_b\rangle = \frac{1}{\sqrt{2\pi 2^{n_b}\, n_b!\,\ell}}\left(\frac{z}{\ell}\right)^{n_b} e^{\ |z|^2/(4\ell^2)}, \qquad n_b = 0, 1, 2, \quad , \tag{34}$$

where $z = r_x \quad ir_y$. These wave functions are peaked at a radius $r_{n_b} = \sqrt{2n_b}\ell$. Also note that any holomorphic function is in the LLL. The filled LLL with N particles is described by the single Slater determinant state

$$_{\mathrm{LLL}}(z_1, \quad , z_N) \ / \ \prod_{i<j}^{N}(z_i \quad z_j)\exp\Big(\quad \sum_{j=1}^{N}\frac{|z_j|^2}{4\ell^2}\Big), \tag{35}$$

with a Vandermonde determinant in front of the exponential term. Laughlin introduced the wave function

$$_m(z_1, \quad , z_N) \ / \ \prod_{i<j}^{N}(z_i \quad z_j)^m \exp\Big(\quad \sum_{j=1}^{N}\frac{|z_j|^2}{4\ell^2}\Big), \tag{36}$$

with m an odd positive integer (for fermions). This wave function describes a state with a reduced density: instead of filling $\nu = 1$ (for $_{\mathrm{LLL}}$), the filling here is $\nu = 1/m$. Correspondingly, the radius of the droplet expands: $r_N \ ! \ r_{mN}$. Furthermore, the term in

front of the exponential induces correlations between the particles so that the minimal relative angular momentum between two particles is equal to m. Remarkably, the elementary excitations are in some sense already contained in the analytic form of the Laughlin wave function. For example, the wave function of a quasihole with fractional charge $1/m$ localized at z_0 is given by

$$ {}^{\mathrm{qh}}_{n}(z_1, \quad , z_N j z_0) \; / \quad {}_{n}(z_1, \quad , z_N) \prod_{l=1}^{N} (z_l \quad z_0). \tag{37} $$

Considering a state with two quasiholes,

$$ j z_0, z_0^{\emptyset} i \qquad {}^{\mathrm{qh}}_{n}(z_1, \quad , z_N j z_0, z_0^{\emptyset}), \tag{38} $$

the braiding of the quasiholes gives a Berry phase of the form $e^{2\pi \mathrm{i}/m}$, i.e., fractional statistics.

From the energetic point of view, the Laughlin state is the highest density zero-energy eigenstate of the positive semidefinite pseudopotential interaction defined by

$$ \widehat{V}^{(m)} = \sum_{l=0}^{m} \sum_{i<j}^{1 \quad N} \widehat{P}_{l;i,j}, \tag{39} $$

where $\widehat{P}_{l;i,j}$ is the projector on the states of particles i and j with relative angular momentum l. In position basis, this potential reads

$$ \widehat{V}^{(m)} = \frac{\partial^{2l}}{\partial (r_i \quad r_j)^{2l}} \delta(r_i \quad r_j). \tag{40} $$

To investigate the presence of a gap, we use the Girvin-MacDonald-Platzman algebra, projecting the bare density operator $\widehat{\rho}_{\mathrm{bare}}(r) = \delta(r \quad \widehat{r})$ on the LLL (or any other Landau level) using the projector $\widehat{P}_0$,

$$ \widehat{\rho}(r) = \widehat{P}_0 \widehat{\rho}_{\mathrm{bare}}(r) \widehat{P}_0. \tag{41} $$

The Fourier components are then

$$ \widehat{\rho}(q) = e^{\mathrm{i} q \, \widehat{x}}, \tag{42} $$

where $\widehat{x}$ is the projected position operator, and obey the commutation relation

$$ \left[\widehat{\rho}(q), \widehat{\rho}(q^{\emptyset}) \right] = \quad 2\mathrm{i} \sin \left(\frac{\ell^2}{2} q \wedge q^{\emptyset} \right) \widehat{\rho}(q + q^{\emptyset}). \tag{43} $$

We perform a variational calculation in the LLL, with the Hamiltonian

$$ \widehat{H}_{\mathrm{LLL}} = \sum_{q} v(q) \delta\widehat{\rho}(q) \delta\widehat{\rho}(\quad q), \tag{44} $$

where

$$ \delta\widehat{\rho}(q) = \widehat{\rho}(q) \quad h\psi_0 j \widehat{\rho}(q) j \psi_0 i \tag{45} $$

is the fluctuation from the ground state expectation value. With the variational state

$$ j\phi(k) i = \delta\widehat{\rho}(k) j \psi_0 i \tag{46} $$

we can compute the excitation energy

$$(k) = \frac{1}{2}\frac{\hbar\psi_0 j\left[\delta\widehat{\rho}(\quad k), \left[\widehat{H}_{\mathrm{LLL}}, \delta\widehat{\rho}(k)\right]\right] j\psi_0 i}{\hbar\psi_0 j\delta\widehat{\rho}(\quad k)\delta\widehat{\rho}(k) j\psi_0 i}. \tag{47}$$

Using the commutator (43) we find the asymptotic behavior

$$(k) \;/\; jkj^4 \quad \text{for} \quad k \;!\; 0. \tag{48}$$

The same behavior can be shown to hold for the Laughlin state. We interpret these results with the existence of a finite gap above the ground state.

We now consider a system on the surface of a torus. The degeneracy of the FQHE ground state for a filling factor $\nu = 1/m$ on a surface of genus g is given by m^g. Therefore, on a torus, the ground state manifold is m-fold degenerate. These ground states are indistinguishable by local operators in the 1D limit: this is the key for topological order. On a thin torus, the FQHE goes into a CDW, with distinguishable states when $L_x \quad \ell$. The "root configuration" states for $m = 3$ are

$$1\ 0\ 0\ 1\ 0\ 0\ 1\ 0\ 0 \tag{49}$$
$$0\ 1\ 0\ 0\ 1\ 0\ 0\ 1\ 0 \tag{50}$$
$$0\ 0\ 1\ 0\ 0\ 1\ 0\ 0\ 1 \tag{51}$$

In addition to the states at $\nu = 1/m$, there are many more FQHE states at other fractional filling factors. The elementary excitations in some of them are thought to obey non-Abelian statistics. The o□-diagonal resistivity response $\sigma_{xy} = \nu e^2/h$ shows a precise fractional quantization at filling factor ν. The edges of a FQHE sample consist of chiral channels carrying fractional quasiparticles.

2.2 Fractional Chern Insulators (FCIs)

Landau levels and a magnetic field are not necessarily needed for the realization of the FQHE. In fact, FCIs arise for flat Chern bands with repulsive short-range (density-density) interactions, described by the Hamiltonian

$$\widehat{H} = \sum_{\boldsymbol{k}}\sum_{a}\varepsilon_a(k)\widehat{c}^{\dagger}_{\boldsymbol{k},a}\widehat{c}_{\boldsymbol{k},a} + \sum_{\boldsymbol{k},\boldsymbol{k}',\boldsymbol{q}}\sum_{\alpha,\beta}V^{\alpha\beta}_{\boldsymbol{q}}\,\widehat{c}^{\dagger}_{\boldsymbol{k}+\boldsymbol{q},\alpha}\widehat{c}^{\dagger}_{\boldsymbol{k}'\ \ \boldsymbol{q},\beta}\widehat{c}_{\boldsymbol{k}',\beta}\widehat{c}_{\boldsymbol{k},\alpha}, \tag{52}$$

where the first (second) term is written using operators for the band basis (local orbital basis), labeled by latin (greek) letters. The change of basis is given by

$$\widehat{c}_{\boldsymbol{k},a} = \sum_{\alpha} u_{\boldsymbol{k},a;\alpha}\widehat{c}_{\boldsymbol{k},\alpha}, \tag{53}$$

where $u_{\boldsymbol{k},a;\alpha}$ is the k-periodic part of the Bloch vector. We now project to one band with non-vanishing Chern number (C 6= 0), e.g., the lower band of Haldane's model, and spectrally flatten the band ($\varepsilon_1(k)$! const): this introduces exponentially decaying hopping amplitudes in real space. The flattened Hamiltonian is

$$\widehat{H}_{\text{at}} = \sum_{\boldsymbol{k},\boldsymbol{k}',\boldsymbol{q}}\sum_{\alpha,\beta}V^{\alpha\beta}_{\boldsymbol{q}}\,(u_{\boldsymbol{k}+\boldsymbol{q};\alpha}u_{\boldsymbol{k};\alpha})(u_{\boldsymbol{k}'\ \ \boldsymbol{q};\beta}u_{\boldsymbol{k}';\beta})\widehat{c}^{\dagger}_{\boldsymbol{k}+\boldsymbol{q}}\widehat{c}^{\dagger}_{\boldsymbol{k}'\ \ \boldsymbol{q}}\widehat{c}_{\boldsymbol{k}'}\widehat{c}_{\boldsymbol{k}}, \tag{54}$$

where we did not write the band index ($a = 1$) on the Bloch amplitudes and ladder operators. In this Hamiltonian, the interactions are weighted by Bloch states factors. As a consequence, topological physics enters through the Bloch states $|u_{\boldsymbol{k}}\rangle$.

We consider now FCIs in the context of quantum geometry. The quantum geometric tensor is

$$Q_{ij}(\boldsymbol{k}) = \langle\partial_{k_i} u(\boldsymbol{k})|\partial_{k_j} u(\boldsymbol{k})\rangle - \langle\partial_{k_i} u(\boldsymbol{k})|u(\boldsymbol{k})\rangle\langle u(\boldsymbol{k})|\partial_{k_j} u(\boldsymbol{k})\rangle \quad (55)$$

$$g_{ij}(\boldsymbol{k}) - \frac{i}{2}F_{ij}(\boldsymbol{k}), \quad (56)$$

where g_{ij} is the (symmetric) Fubini-Study metric, while

$$F_{ij} = i\left[\langle\partial_{k_i} u(\boldsymbol{k})|\partial_{k_j} u(\boldsymbol{k})\rangle - \langle\partial_{k_j} u(\boldsymbol{k})|\partial_{k_i} u(\boldsymbol{k})\rangle\right] \quad (57)$$

is the (antisymmetric) Berry curvature. We note that

$$\langle u(\boldsymbol{k})|u(\boldsymbol{k}+d\boldsymbol{k})\rangle \simeq 1 - \frac{1}{2}g_{ij}(\boldsymbol{k})dk_i dk_j \quad (58)$$

measures the distance between $|u\rangle$ at different $\boldsymbol{k}$ points. The "trace condition" states that

$$\mathrm{tr}[g_{ij}(\boldsymbol{k})] \geq |F(\boldsymbol{k})|, \quad (59)$$

and the "determinant condition" is

$$\det[g_{ij}(\boldsymbol{k})] \geq \frac{1}{4}|F(\boldsymbol{k})|^2. \quad (60)$$

The properties of Landau levels and Bloch bands are summarized in the following table.

	Landau levels	Bloch bands
dispersion	zero	finite
topology	$\lvert C\rvert = 1$	$C \in \mathbb{Z}$
quantum geometry	(59) (60) saturated g_{ij}, F_{ij} $\boldsymbol{k}$-independent	(59) (60) satisfied (for a single band) g_{ij}, F_{ij} $\boldsymbol{k}$-dependent

As a consequence we obtain the commutator for the projected density operators $\hat{\rho}_{\boldsymbol{q}}$

$$\left[\hat{\rho}(\boldsymbol{q}), \hat{\rho}(\boldsymbol{q}')\right] = i(\boldsymbol{q}\wedge\boldsymbol{q}')C\hat{\rho}(\boldsymbol{q}+\boldsymbol{q}') + O(|\boldsymbol{q}|^3), \quad (61)$$

which, to lowest order in $|\boldsymbol{q}|$, corresponds to the GMP algebra. Furthermore, for the Wannier states localized at the lattice sites $\boldsymbol{R}$,

$$\psi_{\boldsymbol{R};\alpha}(\boldsymbol{r}) = \frac{1}{N}\sum_{\boldsymbol{k}} e^{i\boldsymbol{k}\cdot(\boldsymbol{R}-\boldsymbol{r})}u_{\boldsymbol{k};\alpha}, \quad (62)$$

we obtain the spread functional

$$\langle\psi_{\boldsymbol{0}}|\hat{r}^2|\psi_{\boldsymbol{0}}\rangle - \sum_{\boldsymbol{R}}|\langle\psi_{\boldsymbol{0}}|\hat{r}|\psi_{\boldsymbol{R}}\rangle|^2 \geq \frac{CA_{\mathrm{uc}}}{2\pi}, \quad (63)$$

where A_{uc} is the area of a unit cell. It follows that the Wannier states in Chern bands cannot be exponentially localized: at least in some direction, the decay has to be algebraic.

Finally, we review some evidence for FCIs from numerical studies. FCIs appear at band fillings

$$\nu = \frac{k}{|C|(m \quad 1) + 1} \tag{64}$$

for k, m 2 Z. However, systems at low fillings may be unstable to a Wigner crystal. The results are almost independent of the model: a flat berry curvature and a flat band are favorable for the realization of FCIs. They also arise in the so-called "infinite interaction limit", defined by the limit $V_1 \to \infty$ of the repulsive NN interaction V_1 in the Haldane model (without band projection). The tests for the identification of FCIs states include:

- ground state degeneracy,
- quasi-holes states and their counting,
- ground state Chern number and spectral evolution under flux pumping,
- entanglement spectrum.

In particular, the counting of the quasiholes states involves a mapping from the FQHE momenta (on a torus) to FCI crystal momenta:

$$l = N_y k_x + k_y \quad \text{with} \quad \begin{cases} l = 0, \dots, N_\phi \quad 1, & N_\phi = N_x N_y, \\ k_x = 0, \dots, N_x \quad 1, \\ k_y = 0, \dots, N_y \quad 1. \end{cases} \tag{65}$$

For example, for the Laughlin state at $\nu = 1/3$:

- For $N_\phi = 6$, $N_x = 3$, $N_y = 2$

k_x =	0		1		2				
k_y =	0	1	0	1	0	1			
l =	0	1	2	3	4	5			
GS:	1	0	0	1	0	0	!	$Q_x = 1$	$Q_y = 1$
	0	1	0	0	1	0		$Q_x = 2$	$Q_y = 1$
	0	0	1	0	0	1		$Q_x = 0$	$Q_y = 1$

- For $N_\phi = 8$, $N_x = 4$, $N_y = 2$

k_x =	0		1		2		3	
k_y =	0	1	0	1	0	1	0	1
l =	0	1	2	3	4	5	6	7
GS:	1	0	0	1	0	0	0	0
	1	0	0	0	1	0	0	0
	1	0	0	0	0	1	0	0
	0	1	0	0	1	0	0	0
	0	1	0	0	0	1	0	0
	0	1	0	0	0	0	1	0
	0	0	1	0	0	1	0	0
	0	0	1	0	0	0	1	0
	0	0	1	0	0	0	0	1

We remark that the q quasiholes states can be associated to well-defined momentum sectors.